Journal of Fluids Engineering

Copy of e-mail Notification

Journal of Fluids Engineering Published by ASME
Dear Author,

Congratulations on having your paper accepted for publication in the ASME Journal Program.
Your page proof is available in PDF format from the ASME Proof Download & Corrections site here:
http://115.111.50.156/jw/AuthorProofLogin.aspx?pwd=12b64dc23fb7

Login: your e-mail address
Password: 12b64dc23fb7

Please keep this email in case you need to refer back to it in the future.
You will need Adobe Acrobat Reader software to view the file. This is free software and a download link is provided when you log in to view your proofs.

Responsibility of detecting errors rests with the author. Please review the page proofs carefully and:

1) Answer any queries on the first page "Author Query Form"
2) Proofread any tables and equations carefully
3) Check to see that any special characters have translated correctly

RETURNING CORRECTIONS:
To return corrections, please use the ASME Proof Download & Corrections Submission Site (link above) and provide either:

1. Annotated PDF
2. Text entry of corrections, with line numbers, in the text box provided

Additional files, as necessary, can also be uploaded through the site.

SPECIAL NOTES:
Your Login and Password are valid for a limited time. Please reply within 48 hours. Your prompt attention to and return of page proofs will speed the publication of your work.

For all correspondence, please include your article no. (FE-13-1407) in the subject line.
This e-proof is to be used only for the purpose of returning corrections to the publisher.
If you have any questions, please contact: asme.cenveo@cenveo.com.

Sincerely,
Journal Production Manager

STATEMENT OF EDITORIAL POLICY AND PRACTICE

The Technical Committee on Publications and Communications (TCPC) of ASME aims to maintain a high degree of technical, literary, and typographical excellence in its publications. Primary consideration in conducting the publications is therefore given to the interests of the reader and to safeguarding the prestige of the Society.

To this end the TCPC confidently expects that sponsor groups will subject every paper recommended by them for publication to careful and critical review for the purpose of eliminating and correcting errors and suggesting ways in which the paper may be improved as to clarity and conciseness of expression, accuracy of statement, and omission of unnecessary and irrelevant material. The primary responsibility for the technical quality of the papers rests with the sponsor groups.

In approving a paper for publication, however, the TCPC reserves the right to submit it for further review to competent critics of its own choosing if it feels that this additional precaution is desirable. The TCPC also reserves the right to request revision or condensation of a paper by the author or by the staff for approval by the author. It reserves the right, and charges the editorial staff, to eliminate or modify statements in the paper that appear to be not in good taste and hence likely to offend readers (such as obvious advertising of commercial ventures and products, comments on the intentions, character, or acts of persons and organizations that may be construed as offensive or libelous), and to suggest to authors rephrasing of sentences where this will be in the interest of clarity. Such rephrasing is kept to a minimum.

Inasmuch as specific criteria for the judging of individual cases cannot, in the opinion of the TCPC, be set up in any but the most general rules, the TCPC relies upon the editorial staff to exercise its judgment in making changes in manuscripts, in rearranging and condensing papers, and in making suggestions to authors. The TCPC realizes that the opinions of author and editor may sometimes differ, and hence it is an invariable practice that no paper is published until it has been passed on by the author. For this purpose page proofs of the edited paper are sent to the author prior to publication in a journal. Changes in content and form made in the proofs by authors are followed by the editor except in cases in which the Society's standard spelling and abbreviation forms are affected.

If important differences of opinion arise between author and editor, the points at issue are discussed in correspondence or interview, and if a solution satisfactory to both author and editor is not reached, the matter is laid before the TCPC for adjustment.

Technical Committee on Publications and Communications (TCPC)
Reviewed: 05/2012

AUTHOR QUERY FORM

	Journal: J. Fluids Eng. Article Number: FE-13-1407	Please provide your responses and any corrections by annotating this PDF and uploading it to ASME's eProof website as detailed in the Welcome email.

Dear Author,

Below are the queries associated with your article; please answer all of these queries before sending the proof back to Cenveo. Production and publication of your paper will continue after you return corrections or respond that there are no additional corrections.

Location in article	Query / Remark: click on the Q link to navigate to the appropriate spot in the proof. There, insert your comments as a PDF annotation.
AQ1	Please check change from "Table above" to "Table 2" here.
AQ2	Please provide full page range in Refs. [1], [3], and [7].

Thank you for your assistance.

Water Level Rise Upstream a Permeable Barrier in Subcritical Flow: Experiment and Modeling

R. Martino
CONICET – Grupo de Medios Porosos,
Facultad de Ingeniería,
Univ. de Buenos Aires,
Paseo Colón 850 (1063), Argentina
e-mail: rmartino@fi.uba.ar

A. Paterson
Departamento de Hidráulica,
Facultad de Ingeniería,
Univ. de Buenos Aires,
Paseo Colón 850 (1063), Argentina
e-mail: apaters@fi.uba.ar

M. Piva
Grupo de Medios Porosos,
Facultad de Ingeniería,
Univ. de Buenos Aires,
Paseo Colón 850 (1063), Argentina
e-mail: mpiva@fi.uba.ar

This work addresses the dependence of water depth upstream a permeable barrier, h_1, with discharge per unit channel width, Q/W, in sub-critical flow regime. The barrier, that extends over the entire width of the channel, is composed by smooth cylinders of small aspect ratio vertically mounted on the bottom in a staggered pattern and fully submerged in the flow. The height of the cylinders above the bottom was kept constant for all runs. Several configurations were considered by varying systematically the cylinders diameter, d_v, the number of cylinders per unit area of the bed, or density, m, and the length of the barrier in the stream direction, L_v. A one-dimensional model was developed to predict the observed values of h_1 and to obtain a sound basis taking into account the incidence of Q/W, m, d_v and L_v. This model is based on fluid mechanics equations applied on a finite control volume for the flow in the test section, and it was deduced under simplifying assumptions physically-based. Finally, and based on the experimental results and the model predictions, the mechanical energy losses of the flow are analyzed. The main role played by a dimensionless number R, that takes into account the barrier's resistance to the flow, is highlighted. [DOI: 10.1115/1.4026356]

1 Introduction

The relationship between bed roughness patterns and drag resistance is a key area of research in dynamics of free surface flows. The presence of roughness elements along the bed protruding the bulk flow arise the question of the correlation between geometrical properties of the roughness elements and equivalent roughness height [1,2].

Porous or semipermeable barriers are bed-mounted obstacles, of finite size, conformed as clusters, or arrays, of large resistive elements. It is known that the presence of an object or obstacle of finite length in an open channel flow produces a significant change in the flow structure [3], which can be represented as an extra drag force exerted over the flow. Permeable barriers placed on a stream bed is an active field of research because of its practical relevance. The interest in using vegetative buffer strips, or constructed materials, as conservation measures to reduce fluxes of sediments and/or pollutants from overland flows led to numerous studies on determining the efficiency of such barriers together with the associated increment in flow resistance [4].

A first classification in the study of open channel flows through buffer strips or porous barriers is based on the Froude number of the incident flow $F_1 = U_1/(gh_1)^{1/2}$, where $U_1 = Q/(Wh_1)$ is mean flow velocity and Q, W and h_1 are the flow rate, the channel width and the flow depth upstream the obstacle, respectively. If $F_1 < 1$ the flow regime is called subcritical, while if $F_1 > 1$ is called supercritical.

Most of the research works have been performed in flumes under supercritical flow conditions. In these works, permeable barriers are constructed from resistive elements (vertical cylinders, nails, etc.) that form obstacles networks. They are useful for modeling situations encountered in agricultural uses or soil management (vegetative filters, buffer strips, etc.). An example is the work of Rose et al. [5], where a fixed discharge was forced to pass through a buffer strip composed by long emergent nails. Several bed slopes, S, and different buffer densities (number of nails per unit bed area), N_{nails}, were considered. They reported that the extent of the hydraulic adjustment zone is approximately proportional to the ratio N_{nails}/S and proposed a model, based on momentum theory in finite segment, to predict the water depth throughout the resistive array.

However, there are circumstances where the flow is sub-critical [6] and the resistive elements of the barrier are completely submerged. Furthermore, frequently the flow rate, more than the bed slope, is the variable of interest. This is the case; for example, of some shallow overland flows developed on low bed slopes, where groups of large elements (vegetation, debris, rocks and/or boulders; for example) protrude from the bed [7,8].

In general, when a sub-critical flow impinges on an obstacle mounted on the bed, the water level upstream the obstacle increases to provide the extra force (or the extra energy) to overcome the drag force (or the mechanical energy losses). In turn, for a given discharge, an increase in water depth implies a lesser mean flow velocity. This fact is of great importance during transport of sediment, pollutants and/or nutrients. A zone has been reported to be upstream of a buffer strip of emergent nails densely packed, where a net deposition of solids takes place [9].

In hydraulics, the raising of the water level upstream an obstacle, compared to the unperturbed level, is called backwater effect. The study of this phenomenon, which is highly complex because of the large amount of involved variables, is of great interest for engineers, biologists and ecologists. Indeed, not only the overall shape of the barrier, its size and relative position to the main flow direction, are important, but also its internal structure, since they are composed by a number of resistive single elements grouped in a finite region of the bed. Theoretical interpretations of flow through grass strips are very few [10]. Based on previous works, dealing with a uniform cover of large-roughness elements along the bed [11], it can be expected that the shape and the size of every single constitutive element, as well as their number per unit bed area, or density, m, will play a central role in flow resistance. In the analysis, it should also be included both their relative positions and planimetric distribution along the bed. Those previous works choose smooth rigid circular cylinders, of diameter d_v and

Contributed by the Fluids Engineering Division of ASME for publication in the Journal of Fluids Engineering. Manuscript received July 2, 2013; final manuscript received December 14, 2013; published online xx xx, xxxx. Assoc. Editor: Mark R. Duignan.

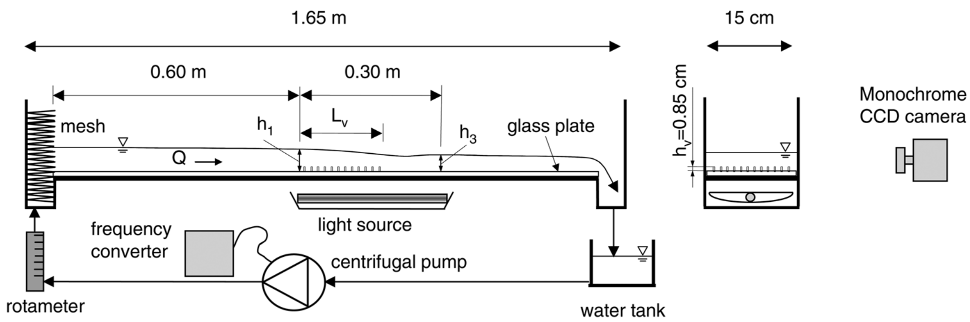

Fig. 1 Scheme of the small horizontal channel and the equipment used for driving and controlling the flow, together with the main dimensions and geometrical variables (not drawn to scale)

of height h_v vertically mounted above the bed in a staggered configuration across the entire width of the channel. In a staggered distribution it is possible to set a desire value of m by simply varying the center-to-center distance of the cylinders, s_v. In addition, the length of the barrier along the stream direction, L_v, should be included in problems of finite barriers.

This experimental contribution addresses the problem of the backwater effect measuring the water depth, h_1, upstream a barrier composed by smooth cylinders, as a function of the flow rate per unit channel width, Q/W. The cylinders, of constant height, were vertically mounted in a staggered pattern. Several configurations were tested by systematically varying the cylinders diameter, d_v, the number of cylinders per unit area of the bed, m, and the barrier's length, L_v. In all cases, the cylinders remained completely submerged in the bulk flow.

Based on fluid mechanics equations under simplifying physically-based assumptions, a one dimensional model is developed to predict the incidence of Q/W, m, d_v and L_v on the observed values of h_1. The dimensionless numbers that appear to play a central role in the mechanics of the phenomenon were identified from this model. An analysis of the implications of these findings on the mechanical energy losses of the flow is finally offered.

2 Experimental Set Up

The experiments were performed in a small 1.65m long and $W = 15$ cm width horizontal open channel with transparent Plexiglas walls (see Fig. 1). The flow was imposed with a centrifugal pump that was controlled with a frequency variator. At the channel inlet, the flow was driven through a honeycomb to ensure a uniform entrance velocity profile. At the channel outlet, the water was allowed to freely discharge in a tank. This outlet flow configuration was preferred to weirs in order to prevent possible interactions between the barrier and the recirculation zone at the upstream side of the weir. Thus, the experiments were designed to avoid additional sources of resistance to flow, so that the increase in the water level is due only to the barrier.

The fluid temperature was registered in all runs, and its values ranged between 24.9 °C and 26.3 °C. Using water as working fluid, the kinematic viscosity of the fluid was $\nu = 0.01\ \mathrm{cm}^2/\mathrm{s}$.

A glass plate 1.50 m long and 15 cm width was placed on the channel floor as a false bottom where the different barriers configurations were mounted. The smoothness of the glass helps to minimize the skin friction, making it insignificant when compared with the barrier's resistance itself (see discussion in Sec. 4). This procedure allows to emphasize the role played by the barrier itself, turning it into the main source of resistance to flow. Of course, in more realistic situations, a friction coefficient should be considered to take into account the presence of grained sediments at the bottom.

The barriers consisted of a network of staggered cylinders of equal height and radius. They were glued with silicon seal on the glass plate to cover a length L_v beginning at 60 cm from the flow inlet, where the flow is assumed to be fully developed, see Fig. 1. Each barrier configuration was constructed following a preprinted pattern in a paper sheet that was located below the glass plate during the preparation process. The staggered configuration was chosen because it has a well defined cylinder's center-to-center distance, and, simultaneously, the longitudinal flow channeling is lower compared with square configurations.

The flow rate, Q, was varied between 1000 l/h to 7000 l/h. Previous measurements for the flow in the test section and in the absence of any barrier (base flow) revealed that the highest water depth (for the maximum tested flow rate) is about 3.0 cm, while the lowest water depth (for the minimum tested flow rate) is about 1.0 cm. Therefore, the flow Reynolds number, based on the mean flow velocity and the channel hydraulic diameter at the test section, varied between 6500 and 37000. The choice of this range of Q will be discussed later, when the drag coefficient for an isolated cylinder and the friction coefficient for a smooth plate are determined. From the above values the flow aspect ratio, W/h_1, varied from 5 to 15. On the other hand, and taking into account the lowest water depth, the height of the cylinders was set at $h_v = 0.85 \pm 0.03$ cm in order to achieve the condition of fully submerged cylinders in all runs.

Two values of s_v were tested, 1.5 cm and 4.5 cm, respectively, see Fig. 2. They ensure that in both cases the barrier width is the same, $W_v = 13.5$ cm, and contain an entire number of cylinders on each row. In turn, in a staggered distribution s_v sets the value

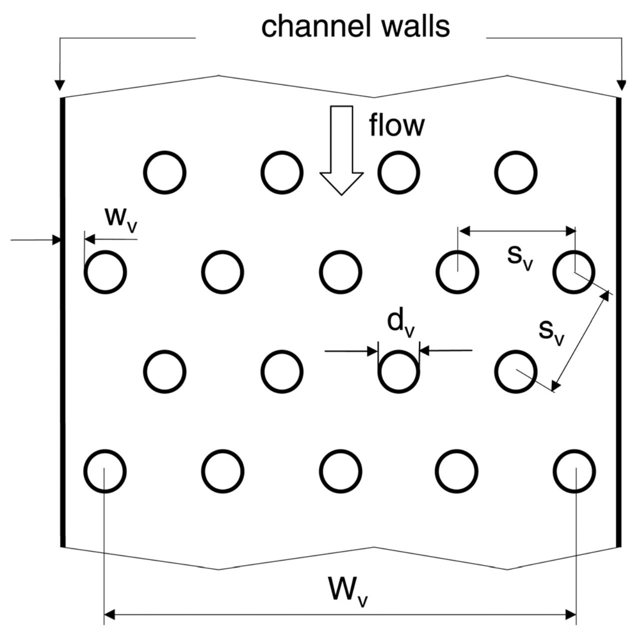

Fig. 2 Plan view of the main geometrical variables for to define the staggered distribution of cylinders (not drawn to scale)

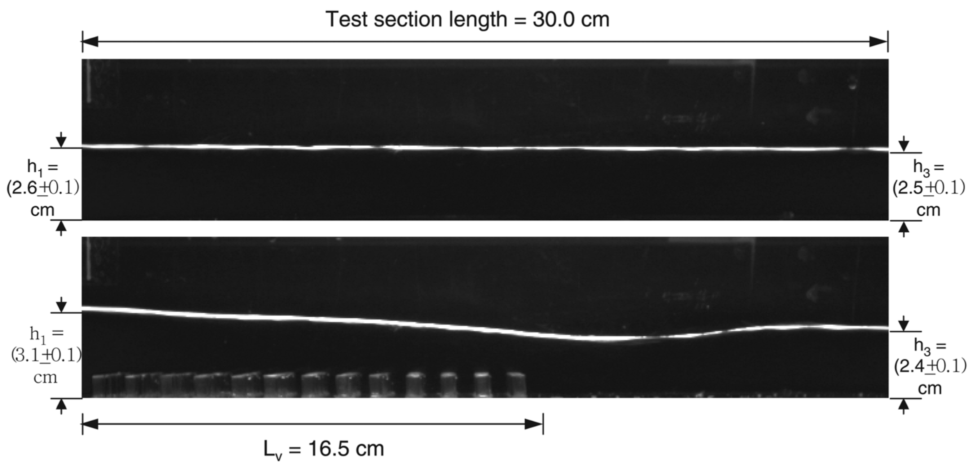

Fig. 3 Two snapshots of the flow at the test section (from left to right), with $Q = 5000\,l/h$ in both cases, showing the differences between the base flow (with no cylinders), in the upper snapshot, and the flow when a barrier is present, with $m = 0.513\,cyls/cm^2$, $d_v = 0.502\,cm$ and $L_v = 16.5\,cm$, in the lower snapshot

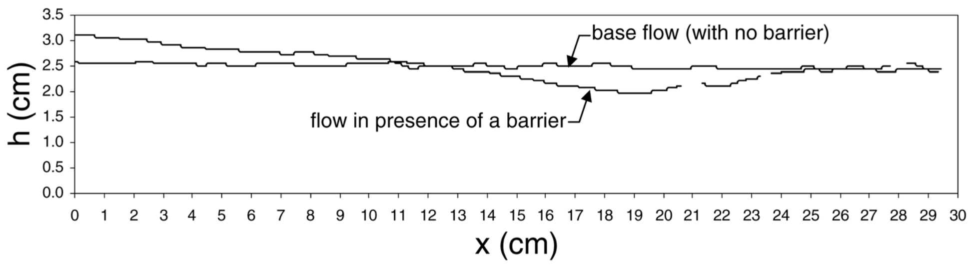

Fig. 4 After analyzing the snapshots showed in Fig. 3 with an ImageJ macro, it is obtained the free surface profile at the test section for both the base flow (no barrier) and for the flow when a barrier is present

of the density, m, defined as $m = (2/\sqrt{3})s_v^{-2}$, which implies m equal to $0.513 cyls/cm^2$ and $0.057 cyls/cm^2$, respectively. The resulting densities are thus separated by almost an order of magnitude.

On the other hand the choice of the cylinders diameter, was guided regarding the barrier solidity ϕ [11], which is defined as $\phi = \pi d_v^2/(4s_v^2)$. This parameter measures the portion of the total bed area that is occupied by cylinders. In order to cover a reasonable wide range of values, two diameters d_v were tested: 0.308 cm and 0.699 cm, respectively, giving $0.03 < \phi < 0.17$.

Recent works on flow over vegetated channels [12] proposed the roughness density $\lambda = d_v h_v / s_v^2$, to quantify the structure of the large roughness cover. If this parameter is much smaller than 0.1, the cover can be considered sparse, whereas if it is much larger than 0.1, the cover is called dense. The case when it is equal to 0.1 is called transitional. From the above, it follows that the tested barriers fall within the range $0.013 \leq \lambda \leq 0.263$.

Finally, three values of L_v were chosen to study the influence of the barrier extension, 3.5 cm, 16.5 cm and 23.0 cm, giving L_v/W ratios less, similar and larger than 1, respectively. In all cases the flow conditions at the channel outlet are not altered with respect to the base flow, for the same discharge.

A Pulnix Dual Tap AccuPixel CCD monochrome camera was placed perpendicular to the lateral side of the channel and centered at the test section (30 cm long, starting at the beginning of the barrier). The free surface was illuminated from below of the bed channel through a light box source with a diffuser plate. By setting the focal plane of the camera on the lateral transparent wall of the channel, it was observed a well-defined bright line corresponding to the water-air-plexiglass contact line, see Fig. 3. It is clear that the water depth corresponds to the lower limit of this bright line. The physical calibration (pixels to centimeters) was obtained by taking a snapshot of a milimetric ruler after each run.

Figure 3(*a*) shows a snapshot of the base flow for $Q = 5000\,l/h$, in absence of the cylinders. Water flows from the left to the right. The free surface is almost flat and the observed slight head loss is due to the friction between the fluid and the smooth walls of the channel.

Figure 3(*b*), shows a snapshot of the flow for the same flow rate Q, but in presence of a barrier. The parameters characterizing the barrier are $m = 0.513\,cyl/cm^2$, $d_v = 0.502\,cm$ and $L_v = 16.5\,cm$. Here, the bright line representing the free surface is markedly affected by the presence of cylinders. The water height at the inlet of the test section, h_1, is larger than the corresponding to the base flow showing the backwater effect upstream the barrier. Accordingly, the free surface slope over the barrier is larger compared to that of the base flow. Immediately downstream the barrier an adjustment zone, with a weak expansion after a *vena contracta* flow region, is observed. Finally, downstream this zone, the flow recovers, and at $x = 30\,cm$ the flow height, h_3, becomes almost the same as in the base flow.

The free surface profile, $h = h(x)$, was extracted by using an ImageJ macro developed to detect the lower bound of the bright line for each snapshot. In Fig. 4 the superposition of the two profiles for the above cases is shown. The impact on the free surface slope due to the barrier's resistance to the water flow is clearly visible. In particular, flow heights at the outlet of the test section (30 cm downstream the inlet) are practically indistinguishable from one case to another.

A summary of the main experimental parameters is given in Table 1.

Table 1 Summary of the variables for the parametric experimental study on the dependence of h_1 with Q

Run	m (cyls/cm^2)	d_v (cm)	L_v (cm)	w_v (cm)
A1	0.513	0.308	16.5	0.6
A2	0.513	0.699	16.5	0.4
B1	0.057	0.502	15.0	0.5
B2	0.513	0.502	16.5	0.5
C1	0.513	0.502	3.5	0.5
C2	0.513	0.502	23.0	0.5

3 Experimental Results

In this section, raw measurements of h_1 as a function of Q/W, for the experimental conditions given in Table 1, are presented. The tests were grouped into three categories: A, B and C, considering the effects of the cylinder diameter, d_v, the density, m and the length barrier, L_v, respectively.

Figure 5 shows the effects of increasing the cylinder diameter. Open squares and open circles correspond to test A1 and A2, respectively. For comparison, the measurements for the base flow (for the same flow rates but with no barrier), are also plotted in black squares. The experimental uncertainties, $\Delta(Q/W)$ /(Q/W) ¡ 10% and $\Delta h_1 = 1$mm, are shown with horizontal and vertical bars in the figures.

It is seen that h_1 grows monotonically and nonlinearly with Q/W for both cylinder diameters and also for the case of no barrier. For a given Q/W, h_1 in presence of the barrier is larger than when there is no barrier, as expected. On the other hand, the larger the diameter of the cylinders, d_v, the larger is the value of h_1.

The results of Test B showing the dependence of h_1 with Q/W for two different densities, m, is shown in Fig. 6. Measurements of the series B1 and B2 are shown in open squares and open circles, respectively, the case of no barrier is shown in filled squares, as above.

The slight difference in L_v values between these configurations is due to the fact that the length of the barrier depends on s_v through $L_v = (\sqrt{3}/2)ns_v$, with n the number of rows. Indeed, $L_v = 16.5$ cm for $s_v = 1.5$ cm is achieved with $n = 13$, but for $s_v = 4.5$ cm the closest value is achieved with $n = 4$ giving $L_v = 15.0$ cm. Beyond this small difference, the same trends can be observed as in the previous case. In particular, for a given Q/W, an increase in the density involves an increase in h_1. Therefore, it can be concluded that not only d_v, but also m, contributes to increase the flow resistance.

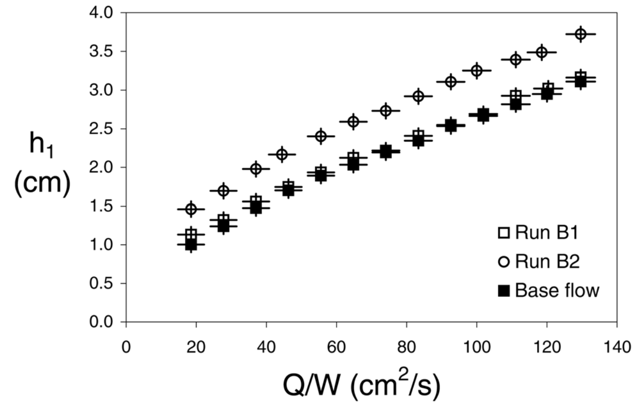

Fig. 6 Effect of barrier density, m, on flow water depth h_1 against discharge per unit channel width, Q/W, for: □ Run B1: m = 0.057 cyls/cm^2 with d_v = 0.502 cm and L_v = 15.0 cm, ○ Run B2: m = 0.513 cyls/cm^2 with d_v = 0.502 cm and L_v = 16.5 cm, and ■ base flow (no barrier)

Figure 7 shows the results of Test C comparing the effects of two different barrier lengths. Open squares correspond to Test C1, open circles are to Test C2, and filled squares for the base flow.

With similar trends as in the previous plots, it is observed that the water level h_1 grows with Q/W in all cases. Also, h_1 is larger than the corresponding value in the base flow configuration when a barrier is present. Finally, for a given Q/W an increase in L_v implies a corresponding increase in h_1.

Therefore, it can be concluded that not only d_v and m, but also L_v is of importance when dealing with flow resistance due to the presence of a permeable barrier, and the corresponding elevation in water depth upstream this barrier.

4 Finite Volume Control Model

This section is devoted to develop a model to predict the increase in water level, h_1, due to the presence of a permeable barrier, for a given flow rate, Q, and water level behind the adjustment zone (downstream the barrier, where flow recovers), h_3 (see Fig. 3). This model is derived from fluid mechanics basic equations (continuity and momentum) using physically based hypothesis.

Let consider a rectangular finite volume control of vertical sides, between locations (1) and (3), as seen in Fig. 3, with the x-axis along the channel bed and the y-axis vertical. Under the

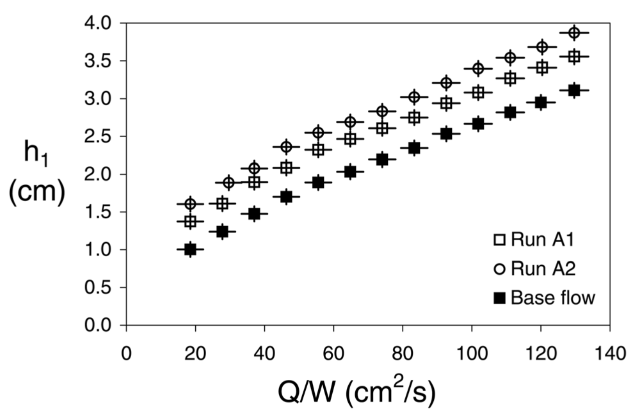

Fig. 5 Effect of cylinders diameter, d_v, on flow water depth h_1 against discharge per unit channel width, Q/W, for: □ Run A1: d_v = 0.308 cm with m = 0.513 cyls/cm^2 and L_v = 16.5 cm, ○ Run A2: d_v = 0.699 cm with m = 0.513 cyls/cm^2 and L_v = 16.5 cm, and ■ base flow (no barrier)

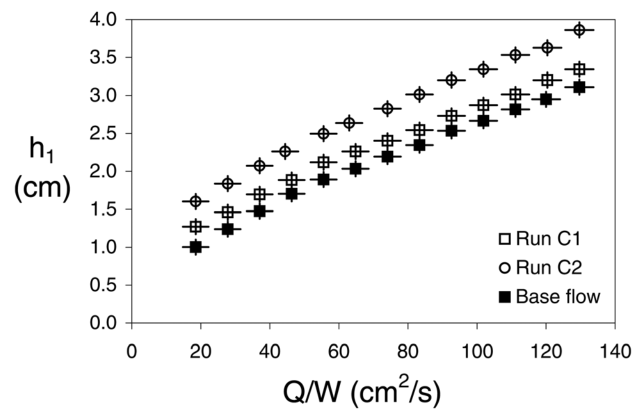

Fig. 7 Effect of barrier length, L_v, on flow water depth h_1 against discharge per unit channel width, Q/W, for: □ Run C1: L_v = 3.5 cm with m = 0.513 cyls/cm^2 and d_v = 0.502 cm, ○ Run C2: L_v = 23.0 cm with m = 0.513 cyls/cm^2 and d_v = 0.502 cm, and ■ base flow (no barrier)

hypothesis of incompressible, stationary and uniform flow at the locations (1) and (3), the integral form of the mass conservation equation can be written as follows:

$$Q = U_1 A_1 = U_3 A_3 \tag{1}$$

where U_1, U_3 and $A_1 = Wh_1$ and $A_3 = Wh_3$ are the mean flow velocities and areas of the control surface at sections (1) and (3), respectively.

Under the assumption of hydrostatic pressure distribution at sections (1) and (3), the Newton's second law of motion (momentum equation) along x, is given by:

$$-D - F_b - \left(\rho g W \frac{h_3^2}{2} - \rho g W \frac{h_1^2}{2}\right) = \rho U_3^2 A_3 - \rho U_1^2 A_1 \tag{2}$$

where g is gravity acceleration, ρ is fluid density, D is the total drag force exerted by the cylinders of the barrier and F_b is the force term associated with glass plate skin friction. The next step is to propose suitable formulations for D and F_b.

First, it is assumed that D can be expressed as the sum of the single drag forces associated with each cylinder. Therefore, D can be written as:

$$D = \sum_{i=1}^{N} C'_d \frac{1}{2} \rho \gamma U_1^2 h_v d_v \tag{3}$$

where $N = mWL_v$ is the number of cylinders forming the barrier and C'_d is the drag coefficient of a single cylinder. Coefficient γ reflects the fact that the velocity impinging each cylinder should not necessarily be equal to the mean velocity, U_1 [13]. A discussion on the values of C'_d and γ will be given later in this section.

Second, F_b is calculated through the Darcy-Weisbach coefficient, f_b, as follows:

$$F_b = f_b \frac{1}{8} \rho \gamma U_1^2 \left(WL_v - N\frac{\pi d_v^2}{4}\right) \tag{4}$$

where the term in parenthesis represents the effective area of the glass plate contributing to flow resistance. As can be noted, the friction force associated with the portion of the glass plate between the end of the barrier $(x = L_v)$ and location (3) $(x = 30\,\text{cm})$ has not been included. In fact, as it will be discussed below, the skin friction of the whole (smooth) glass plate is insignificant with respect to the resistance due to the cylinders.

By replacing Eqs. (3) and (4) in Eq. (2), together with $U_1 = Q/A_1$ and $U_2 = Q/A_2$, and after rearrange terms, it is obtained the following:

$$C'_d \gamma \frac{1}{2} \frac{Q^2}{A_1^2} WL_v \left(md_v h_v + \frac{f_b}{4C'_d}\left(1 - m\frac{\pi d_v^2}{4}\right)\right) = \left(\frac{Q^2}{A_1} + gW\frac{h_1^2}{2}\right) - \left(\frac{Q^2}{A_3} + gW\frac{h_3^2}{2}\right) \tag{5}$$

Therefore, for a given barrier, defined by m, d_v and L_v, and by considering suitable values for γ, C'_d and f_b (all of them having a well definite physical meaning), Eq. (5) implicitly defines h_1 as a function of discharge, Q, and the corresponding water depth downstream, h_3. In principle, the solution for h_1 can be obtained by solving the implicit equation. As an alternative procedure, the both sides of Eq. (5) can be multiplied by h_1^2, and, after rearrange terms, a fourth-order polynomial is obtained:

$$h_1^4 - \left(h_3^2 + \frac{q}{h_3}\right) h_1^2 + q h_1 - \frac{\gamma C'_d}{2} q L_v (md_v h_v + \varepsilon) = 0 \tag{6}$$

with

$$q = \frac{2}{g}\left(\frac{Q}{W}\right)^2 \tag{7}$$

$$\varepsilon = \frac{f_b}{4C'_d}\left(1 - m\frac{\pi d_v^2}{4}\right) \tag{8}$$

Some authors argue that the parameter γ depends on the relative submergence of the cylinder, being less than 1 for fully submerged cylinders within barriers of "infinite" length under uniform flow conditions [11]. These studies do not include the possible dependence of the parameter with the longitudinal position of the cylinders in the channel, x, measured from the point where the barrier begins. Instead, they focus on the asymptotic value of γ, corresponding to values for $x \gg s_v$. Near the beginning of the barrier is reasonable that γ approaches unity as the mean velocity which impinges on the first cylinder is U_1. While more research is needed to examine this issue in depth, as a first approximation to the calculation of the effective drag we consider $\gamma = 1$, which means that all the cylinders are impinged by the same mean flow velocity U_1. The validity of this simplification can be judged by the consistency of the results.

The drag coefficient for a single smooth circular cylinder with infinite aspect ratio (i.e., length $\gg$ diameter) depends on the cylinder's Reynolds number, Re_v, based on the mean velocity of the impinging flow and the diameter of the cylinder. Therefore, strictly speaking, C'_d depends on the actual impinging flow whose depth h_1 is unknown. If, in a first approximation, the base flow is taken as reference, with the extreme values of d_v (see Table 1) is $585 \leq \text{Re}_v \leq 2900$. The available bibliography [14] presents values for C'_d against Re_v for smooth cylinders of aspect ratio $h_v/d_v = 5$, being this values roughly constant for $10^3 \leq \text{Re}_v \leq 10^5$ (and lower than those for cylinders with infinite aspect ratio). In the present work $1.2 \leq h_v/d_v \leq 2.8$, that corresponds to $0.64 \leq C'_d \leq 0.72$ obtained from the above cited reference. Therefore, $C'_d = 0.68 \pm 0.04$ can be considered a representative value for the working conditions. Possible interference effects, that could arise from the proximity of the neighboring cylinders, are not considered.

Regarding friction coefficient associated with the glass plate, f_b, it is assumed the Blasius correlation for turbulent flow in a smooth pipe ([15]; pg. 335) is valid:

$$f_b = \frac{0.3164}{\text{Re}^{0.25}} \tag{9}$$

where the Reynolds number, Re, in the above equation, was taken as equal to those corresponding to the base flow previously discussed (see Sec. 2), which ranges between 6500 and 37000, then $f_b = 0.027 \pm 0.004$ is the average value in this range. This last result made the term ε in Eq. (6) of about one order of magnitude less than $md_v h_v$ (see Table 1) except for run B1, where it is still $\varepsilon < md_v h_v$ but of the same order of magnitude. Therefore, it can be assumed that, in most of the configurations, ε can be neglected in a first approximation.

The latter result depends on the initial assumption to model the force F_b via Eq. 4. If the false bottom is described as a smooth flat plate, the corresponding drag resistance can be approximated as $C_{Db} 1/2 \rho U_1^2 WL_v$, where C_{Db} is the drag coefficient for a flat plate at zero incidence [16]. The Reynolds number based on the mean velocity of the base flow and the test section length (30 cm) varies between 60,000 and 130,000, therefore, from the cited reference, C_{Db} lies in the range $0.01 \leq C_{Db} \leq 0.013$. After substituting in Eq. (2) is obtained that the ratio of C_{Db}/C'_d is negligible when compared to the term $md_v h_v$. This reinforces the conclusion of the previous paragraph.

For each run, roots of the polynomial were numerically computed and were only considered those with physical meaning (real, positive and in the subcritical flow regime). Direct comparison between measurements and model predictions are shown in Figs. 8 and 9 and 10. The good agreement indicates that the model

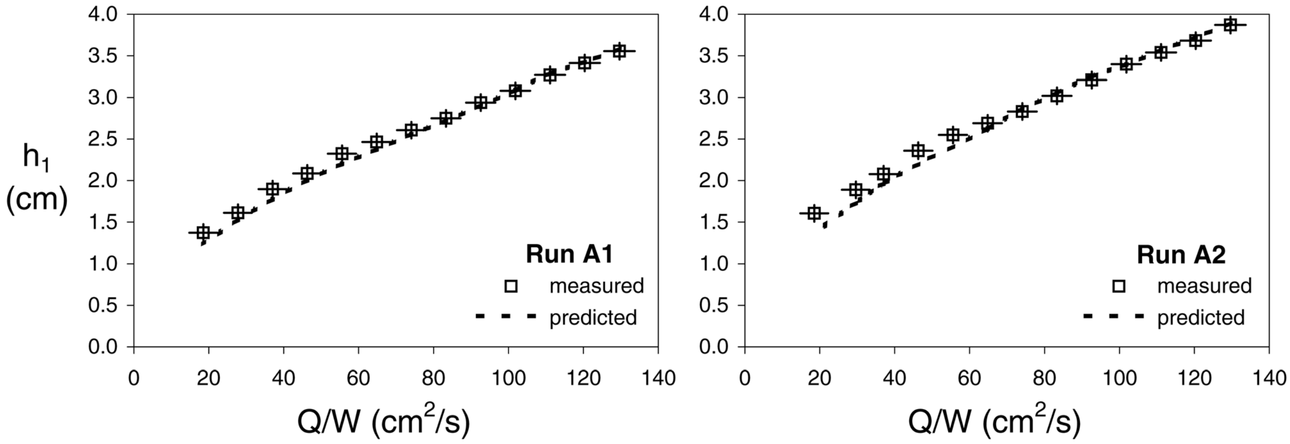

Fig. 8 Comparison between measured (□, repeated) and computed (- - -, Eq. (6)) h_1 against Q/W, for two cylinder diameters, d_v: Run A1: $d_v = 0.308$ cm with m = 0.513 cyls/cm^2 and $L_v = 16.5$ cm; and Run A2: $d_v = 0.699$ cm with m = 0.513 cyls/cm^2 and $L_v = 16.5$ cm

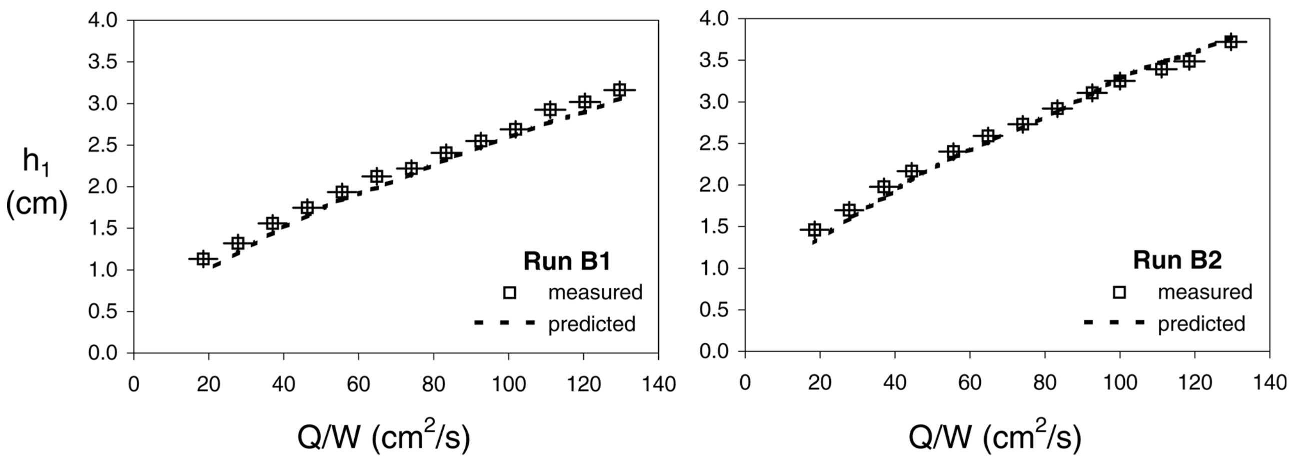

Fig. 9 Comparison between measured (□, repeated) and computed (- - -, Eq. (6)) h_1 against Q/W, for two barrier densities, m: Run B1: m = 0.057 cyls/cm^2 with $d_v = 0.502$ cm and $L_v = 15.0$ cm; and Run B2: ○ m = 0.513 cyls/cm^2 with $d_v = 0.502$ cm and $L_v = 16.5$ cm

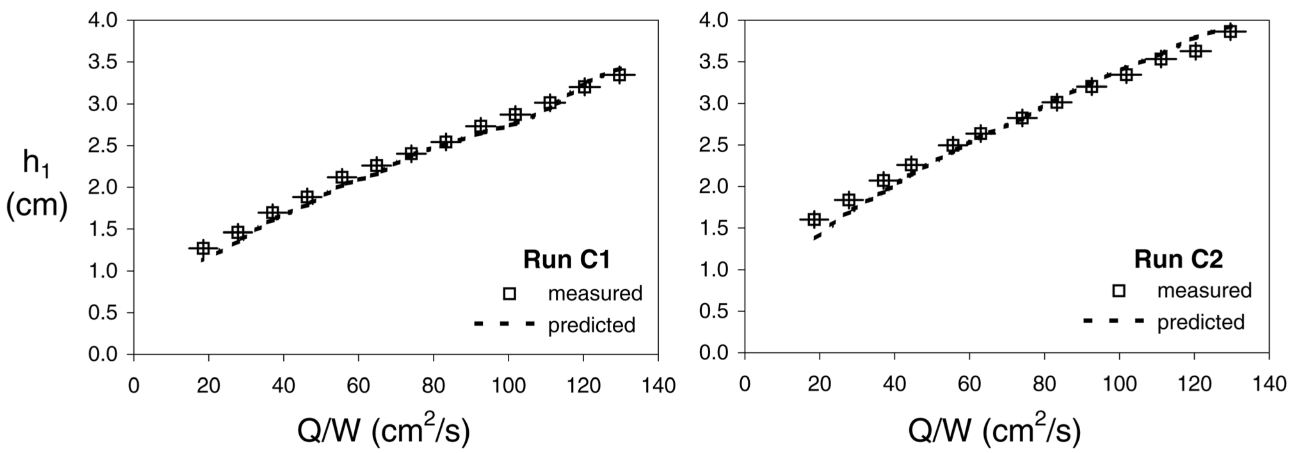

Fig. 10 Comparison between measured (□, repeated) and computed (- - -, Eq. (6)) h_1 against Q/W, for two barrier lengths, L_v: Run C1: $L_v = 3.5$ cm with m = 0.513 cyls/cm^2 and $d_v = 0.502$ cm; and Run C2: $L_v = 23.0$ cm with m = 0.513 cyls/cm^2 and $d_v = 0.502$ cm

certainly captures the dependence of h_1 with Q/W, even with the rough approximations that were made.

The results suggest that, at first order, the working hypothesis $\gamma = 1$ provides the appropriate velocity scale for the mean flow inside the space occupied by the barrier. Future research about this point is needed, taking into account the several simplifications introduced in the model.

Beyond this, it is observed that Eq. (6) is sensitive to the different values of barrier control variables, d_v, m and L_v, in the sense that changes of these variables were captured in predicted values.

Table 2 Summary of the new set of values of d_v, m and L_v, together with those previously discussed

Run	m (cyls/cm^2)	d_v (cm)	L_v (cm)	md_vL_v
A1	0.513	0.308	16.5	2.6
A2	0.513	0.699	16.5	5.9
B1	0.057	0.502	15.0	0.4
B2	0.513	0.502	16.5	4.3
C1	0.513	0.502	3.5	0.9
C2	0.513	0.502	23.0	5.9
D1	0.513	0.502	10.2	2.6
D2	0.513	0.699	10.2	3.7
D3	0.513	0.699	3.5	1.3
D4	0.513	0.308	23.0	3.6
D5	0.513	0.308	10.2	1.6
D6	0.513	0.308	3.5	0.6
D7	0.128	0.502	15.0	1.0

Furthermore, Eq. (6) shows that the predicted value of h_1 does not depends only on Q/W and h_3, but also on the parameter $md_vh_vL_v$. This parameter combines the internal structure of the resistive barrier with its whole size. The results suggest that this parameter could be useful in classifying different barriers.

In order to provide more robustness to the above analysis and test the predictive ability of the model, a new set of measurements of h_1 was performed by combining the variables m, d_v and L_v, for the same range of Q/W previously considered. In Table 2 the new set is designed by D1 to D7.

AQ1 The last column in Table 2 corresponds to the parameter md_vL_v. Similar values for this parameter were obtained by combining different values of m, d_v and/or L_v. For example, run D1 with A1, D7 with C1, and D4 with D2. Furthermore, intermediate values were tested between the previously analyzed; for example for run D2, between runs A1 and B2, or run D6 between B1 and C1.

Figure 11 shows the correlation plot between measured and predicted values of h_1. Again, and taking into account the approximations in the model, it is observed that the agreement between them is quite good. A slight deviation in the lower part of the perfect agreement curve is observed, indicating that theoretical values slightly underestimate the experimental ones in the range of low flow rates.

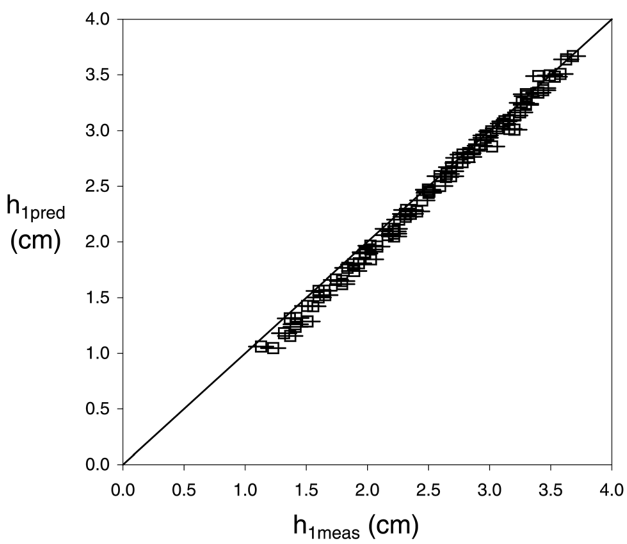

Fig. 11 Direct comparison between measurements, h_{1meas}, and the corresponding predicted value from Eq. (6), h_{1pred}, for the new set of measurements D1 to D7 (see Table 2). Continuous line shows perfect agreement.

By setting the reference length scale equal to the downstream water depth, h_3, a nondimensional equation can be obtained by dividing both sides of Eq. (6) by h_3^4 and considering f_b negligible:

$$\eta^4 - \left(1 + 2F_3^2\right)\eta^2 + 2F_3^2\eta - 2F_3^2R = 0 \quad (10)$$

where $\eta = h_1/h_3$ is the water depth at section (1) relative to the water level at section (3). In obtaining Eq. (10) the Froude number at section (3) arises naturally from its definition, $F_3 = U_3/(gh_3)^{1/2}$, and the following relationship:

$$\frac{q}{h_3^3} = \frac{2Q^2}{gW^2h_3^3} = \frac{2}{gh_3}\left(\frac{Q}{Wh_3}\right)^2 = 2F_3^2 \quad (11)$$

Finally, R is a nondimensional parameter related to the barrier resistance to the impinging flow, defined as:

$$R = \frac{\gamma C_d'}{2}\frac{md_vL_vh_v}{h_3} \quad (12)$$

Equation (10) implicitly gives the value of η as a function of F_3 and R. For a given F_3, the roots of this equation will provide the values of η as a function of R. From the measurements can be calculated $F_3 = 0.77$ as the average value, with a standard deviation $\Delta F_3 = 0.09$. Therefore, because of the narrow range explored by F_3, it can be expected a grouping effect of the data in the plane $\eta - R$. Figure 12 shows that this is the case for all the experimental points, together with a continuous curve that corresponds to the roots of Eq. (10), obtained numerically by setting $F_3 = 0.77$.

As can be seen, most of the points are grouped around this continuous curve. The graph shows that η monotonically increases with increasing R. The grouping effect is explained by the fact that an increase in Q/W also implies an increase of h_3, resulting F_3 approximately constant through the present runs.

5 Mechanical Energy Dissipation Due to a Permeable Barrier

This section discusses the mechanical energy losses that occur in subcritical flows through permeable barriers, focusing on the function of the resistance number R previously defined. Under the same assumptions as above, the First Law of Thermodynamics (energy equation) applied to the control volume defined in Fig. 1 is write as:

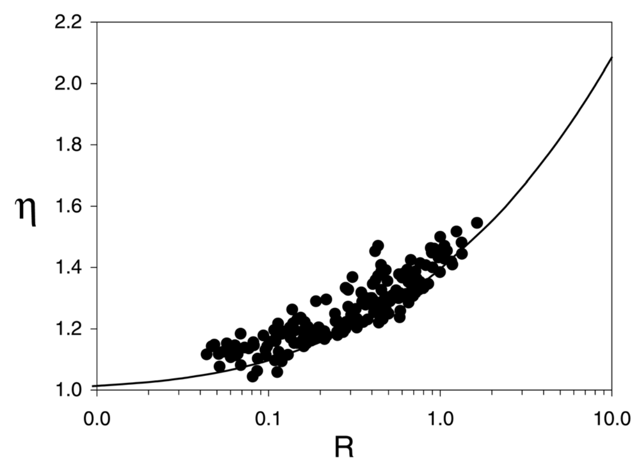

Fig. 12 The dimensionless flow depth $\eta = h_1/h_3$ as a function of the resistance parameter $R = (\gamma C_d'/2)md_vL_vh_v/h_3$, for all the downstream Froude numbers, F_3, Runs A_1 to D_7. Continuous line corresponds to the average value $F_3 = 0.77$, with standard deviation $\Delta F_3 = 0.09$.

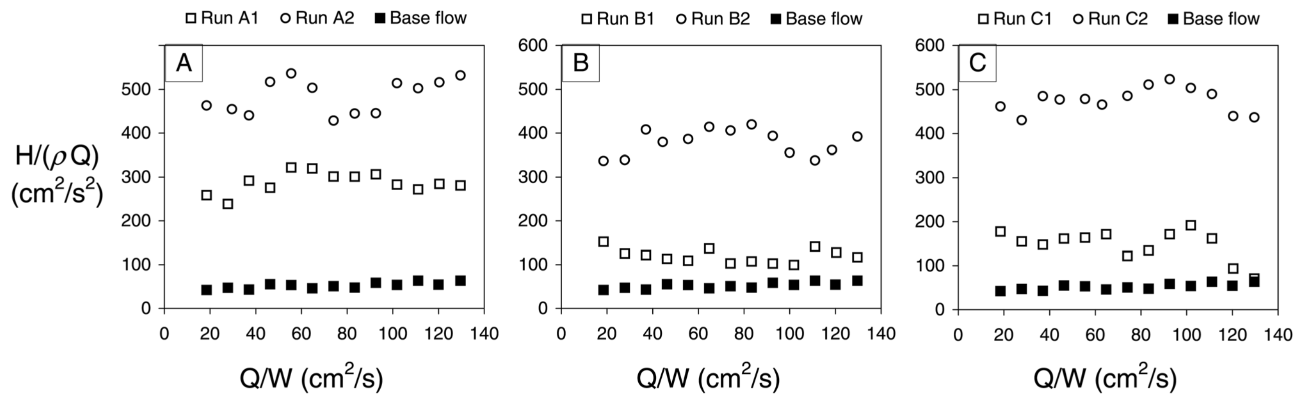

Fig. 13 Specific mechanical energy losses, $H/(\rho Q)$, against discharge per unit channel width, Q/W: (*a*) influence of cylinder diameter, d_v, for $m = 0.513$ cyls/cm^2 and $L_v = 16.5$ cm, □ $d_v = 0.308$ cm and ○ $d_v = 0.699$ cm; (*b*) influence of barrier density, m, for $d_v = 0.502$ cm and $L_v = 15.0$ cm, □ $m = 0.057$ cyls/cm^2 and ○ $m = 0.513$ cyls/cm^2; (*c*) influence of barrier length, L_v, for $m = 0.513$ cyls/cm^2 and $d_v = 0.502$ cm, □ $L_v = 3.5$ cm and ○ $L_v = 23.0$ cm. ■ base flow, $md_vL_v = 0$ cm. Uncertainties bars for $H/(\rho Q)$ are of the order of data fluctuations and are not plotted for clarity.

$$\left(\frac{U_1^2}{2} + gh_1\right) = \left(\frac{U_3^2}{2} + gh_3\right) + \left((u_3 - u_1) - \frac{\dot{\phi}}{\rho Q}\right) \tag{13}$$

where g is the acceleration of gravity, ρ is the fluid density, $U_1 = Q/(Wh_1)$ and $U_3 = Q/(Wh_3)$ are the uniform flow velocities at sections (1) and (3), $(u_3 - u_1)$ is the increment in internal energy per unit mass of fluid and $\dot{\phi}/(\rho Q)$ is the heat transferred to the surroundings per unit mass of fluid.

The term $(u_3 - u_1) - \dot{\phi}/(\rho Q) = H/(\rho Q)$ represents an irreversible loss of mechanical energy per unit mass of the fluid due to viscous dissipation, resulting in a conversion of mechanical energy into internal energy (not recoverable) and in heat transferred to the surroundings. The Second Law of Thermodynamics (entropy equation) imposes that $H > 0$. In terms of H, Eq. (13) can be rewritten as follows:

$$\left(\frac{U_1^2}{2} + gh_1\right) - \left(\frac{U_3^2}{2} + gh_3\right) = \frac{H}{\rho Q} \tag{14}$$

The left hand side of Eq. (14) can be evaluated from experimental values of mean velocity and water depth in sections (1) and (3) to obtain $H/(\rho Q)$ as a function of the flow rate Q/W for different barrier parameters combinations.

With the same notation as in the previous analysis (Fig. 13) shows the evolution of $H/(\rho Q)$ with Q/W for runs A, B and C (see Table 1 for input parameters). Open and filled markers correspond to $H/(\rho Q)$ in the presence of the barrier and for the base flow configuration, respectively. Data points have large uncertainties (not shown for clarity), as a result of the way in which $H/(\rho Q)$ is calculated from Eq. (14). Beyond this fact, the overall picture that emerges is that an increase in barrier resistance (via an increment in d_v, m or L_v) is followed by an increase in $H/(\rho Q)$, regardless the values of Q/W.

The above paragraph suggests that $H/\rho Q$ mainly depends on the resistance offered by the barrier. From the preceding section the dimensionless number R is representative of this resistance. On the other hand, a dimensionless number $H^* = H/(\rho Q g h_3)$ naturally arises by dividing Eq. (14) by gh_3.

Figure 14 shows the trend of H^* when plotted against R for all the experimental data. A remarkable grouping effect in the whole explored range, is observed. Moreover, a linear relationship between H^* and R is compatible, where the ordinate intercept represents H^* for the flow in absence of a barrier (i.e., $R = 0$).

This result implies that, for a given barrier, the mechanical energy of the flow that is being dissipated per unit time, H, is proportional to the mass flow rate, ρQ, and the flow depth downstream of the adjustment zone, h_3, through the barrier structure

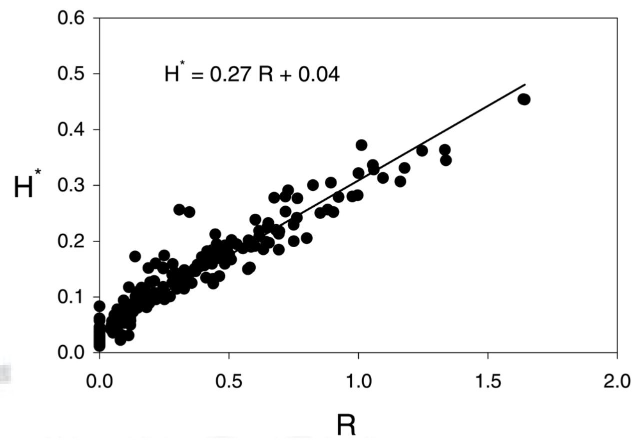

Fig. 14 Dependence of H^* with R (for $\gamma = 1$ and $C'_d = 0.68$)

parameter, R. Indeed, it should be emphasized the key role played by this parameter, it encompasses the main information needed to characterizing a submerged barrier from the point of view of flow resistance. In practice, the value of R gives a suitable criterion for the classification of different permeable barriers and for that reason constitute a useful alternative tool to estimate the backwater effect. Interesting to note is that R can be expressed as the product of a drag coefficient of a single element, C'_d, by a dimensionless factor, $md_vh_vL_v/h_3$, that plays an analog role to the blockage ratio defined by Azinfar and Kells [17] in his study of the backwater effect due to the presence of spur dikes.

6 Conclusions

This contribution experimentally explores the dependence of the water depth upstream a permeable barrier, h_1, with the discharge per unit channel width, Q/W. Experiments are carried out in a small horizontal channel with smooth walls. The permeable barrier extends over the entire width of the channel and it is composed of smooth cylinders of small aspect ratio, vertically mounted in staggered pattern over a smooth glass plate (false bottom). Cylinders height above the bottom is kept constant for all runs, and they are fully submerged in the bulk flow in all cases. Flow is steady and sub-critical, and discharges free at the outlet of the channel.

Several configurations were considered by systematically varying the diameter of the cylinders, d_v, the density of elements per unit area of the bottom, m, and the length of the barrier in the stream direction, L_v. Measurements without the barrier (base flow) were also performed as reference case.

In first place, in all cases it was observed that h_1 grows monotonically with Q/W, both for the base flow case (no barrier) as well as in presence of the resistive barrier. In second place, when water flows in presence of a barrier, the measured values for h_1 are larger than those measured in the base flow configuration. Finally, for a constant Q/W it is observed that h_1 increases with increased values of d_v, m and/or L_v.

A one-dimensional model is presented, based on fluid mechanics equations applied to a finite control volume in the test section, under simplifying assumptions physically-based. The objectives are to predict h_1 and to obtain a sound basis taking into account the quantitative incidence of Q/W, m, d_v and L_v. The contribution to the flow resistance, due to the barrier, was modeled by a net drag force which is equal to the sum of each term of drag over an isolated smooth cylinder of finite aspect ratio. The mean velocity of the impinging flow is postulated to be equal to the mean velocity of the bulk flow immediately upstream the barrier, U_1 (parameter $\gamma = 1$). It is assumed that the contribution to flow resistance from the smooth glass plate (false bottom), where cylinders are mounted, is negligible in first approximation. This assumption is explicitly made in the model, after considering the relative weights of the two contributions to the flow resistance.

Beyond this rough approximations, the model captures the observed trend of h_1 along the explored range of Q/W. Additionally, the model is sensitive to the changes of the control variables of the barrier, d_v, m and L_v, being those changes captured in the predicted values for h_1. It is interesting to note that the fairly good agreement between predictions and measurements is obtained by assuming that all the cylinders are impinged by the same mean flow velocity, U_1,.

The dimensionless momentum equation, via the length scale h_3, implicitly gives $\eta = h_1/h_3$ as a function of two dimensionless numbers: the Froude number downstream de adjustment zone, F_3, where the flow recovers, and the dimensionless resistance parameter, R. From the measured data it is obtained the averaged value $F_3 = 0.77$, with standard deviation $\Delta F_3 = 0.09$, therefore it is assumed that η mainly depends on R for these flow configuration under study. By plotting the measured data in terms of η and R, it is observed that the values are grouped and follow the predicted trend in the plane $\eta - R$, by setting $F_3 = 0.77$ in Eq. (10).

Finally, an analysis about the implications of these findings on the mechanical energy dissipation of the flow are offered. From the measurements it is obtained that the mechanical energy losses per unit mass of the fluid, $H/(\rho Q)$, does not follow any definite trend with Q/W, but increases with d_v, m and/or L_v. By assuming that h_3 is the suitable length scale, it is showed that $H^* = H/(\rho Q g h_3)$ grows fairly linearly with R. This result reinforces the main role played by R in flow resistance, in the sense that the mechanical energy dissipation per unit time depends, besides the flow rate and the downstream flow depth, as seen on both local and global scales of the permeable barrier.

Nomenclature

$A_1 = Wh_1$
$A_3 = Wh_3$
C'_d = drag coefficient for an smooth isolated cylinder of small aspect ratio
d_v = cylinder's diameter
D = total drag force exerted by the cylinders of the barrier
$F_1 = U_1/(gh_1)^{1/2}$
$F_3 = U_3/(gh_3)^{1/2}$
F_b = friction force associated with the smooth false bottom (glass plate)
f_b = Darcy-Weisbach friction coefficient
g = gravity acceleration
H = mechanical energy losses per unit time
$H^* = H/(\rho Q g h_3)$
h_1 = flow depth at the inlet of the test section (immediately upstream the permeable barrier)
h_3 = flow depth at the outlet of the test section (behind the adjustment zone downstream the barrier)
L_v = length of the permeable barrier in the longitudinal direction
m = cylinders density (number of cylinders per unit area of the bottom)
$N = mWL_v$
Q = flow rate
$q = 2/g(Q/W)^2$
$\mathrm{Re}_v = \gamma U_1 d_v/\nu$
$R = (\gamma C'_d/2)(m d_v L_v h_v/h_3)$
s_v = cylinder's center-to-center distance
$U_1 = Q/A_1$
$U_3 = Q/A_3$
W = channel width (= 15 cm)
W_v = barrier width (= 13.5 cm)
w_v = distance between channel walls and neighboring cylinders
γ = coefficient that reflects the fact that the velocity impinging each cylinder should not necessarily be equal to the mean velocity U_1, in a first approximation is assumed to be $\gamma = 1$
$\varepsilon = (f_b/(4C'_d))(1 - m\pi d_v^2/4)$
$\eta = h_1/h_3$
$\lambda = d_v h_v/s_v^2$
ν = fluid kinematic viscosity
ρ = fluid density
$\phi = \pi d_v^2/(4s_v^2)$

References

[1] Flack, K. A., and Schultz, M. P., 2010, "Review of Hydraulic Roughness Scales in the Fully Rough Regime," ASME J. Fluids Eng., **132**, pp. 041203–■. AQ2
[2] Huthoff, F., 2012, "Theory for Flow Resistance Caused by Submerged Roughness Elements," J. Hydraul. Res., **50**(1), pp. 10–17.
[3] Ikram, Z., Avital, E. J., and Williams, J. J. R., 2012, "Detached Eddy Simulation of Free-Surface Flow Around a Submerged Submarine Fairwater," ASME J. Fluid Eng., **134**(6), pp. 061103–■.
[4] Muñoz-Carpena, R., Parsons, J., and Wendell Gilliam, J., 1999, "Modeling Hydrology and Sediment Transport in Vegetative Filter Strips," J. Hydrology, **214**(1–4), pp. 111–129.
[5] Rose, C. W., Hogarth, W., Ghadiri, H., Parlange, J., and Okoma, A., 2002, "Overland Flow to and Through a Segment of Uniform Resistance," J. Hydrology **255**(1–4), pp. 134–150.
[6] Hussein, J., Yu, B., Ghadiri, H., and Rose, C., 2007, "Prediction of Surface Flow Hydrology and Sediment Retention Upslope of a Vetiver Buffer Strip," J. Hydrology, **338**(1–4), pp. 261–272.
[7] Canovaro, F., Paris, E., and Solari, L., 2007, "Effects of Macro-Scale Bed Roughness Geometry on Flow Resistance," Water Resource Res., **43**, pp. W10414–■.
[8] Chen, X., and Chiew, Y., 2003, "Response of Velocity and Turbulence to Sudden Change of Bed Roughness in Open-Channel Flow," J. Hydraul. Eng., **129**(1), pp. 35–43.
[9] Rose, C., Yu, B., Hogarth, W., Okom, A., and Ghadiri, H., 2003, "Sediment Deposition From Flow at Low Gradients into a Buffer Strip – A Critical Test of Re-Entrainment Theory," J. Hydrology, **280**(1–4), pp. 33–51.
[10] Ghadiri, H., and Rose, C. W., 2006, "Grass Strip Hydrology," *Encyclopedia of Soil Science*, Taylor & Francis, London, pp. 773–776.
[11] Stone, B., and Shen, H., 2002, "Hydraulic Resistance of Flow in Channels With Cylindrical Roughness," J. Hydraul. Eng., **128**(5), pp. 500–506.
[12] Nepf, H., 2012, "Flow and Transport in Regions With Aquatic Vegetation," Ann. Rev. Fluid Mech., **44**, pp. 123–142.
[13] Fenton, J. D., 2003, "The Effects of Obstacles on Surface Levels and Boundary Resistance in Open Channels," Proc. 30th IAHR Congress, J. Ganoulis, and P. Prinos, eds., Vol. C2, pp. 9–16.
[14] White, F. M., 2003, *Fluid Mechanics*, McGraw-Hill, New York.
[15] Fox, R. W., and McDonald, A. T., 1994, *Introduction to Fluid Mechanics*, Wiley, New York.
[16] Schlichting, H., and Gersten, K., 2000, *Boundary Layer Theory*, 8th ed., Springer, New York, pp. 583–584.
[17] Azinfar, H., and Kells, J. A., 2011, "Drag Force and Associated Backwater Effect Due to an Open Channel Spur Dike Field," J. Hydraul. Res., **49**(2), pp. 248–256.